SUPPLEMENTARY FIGURES

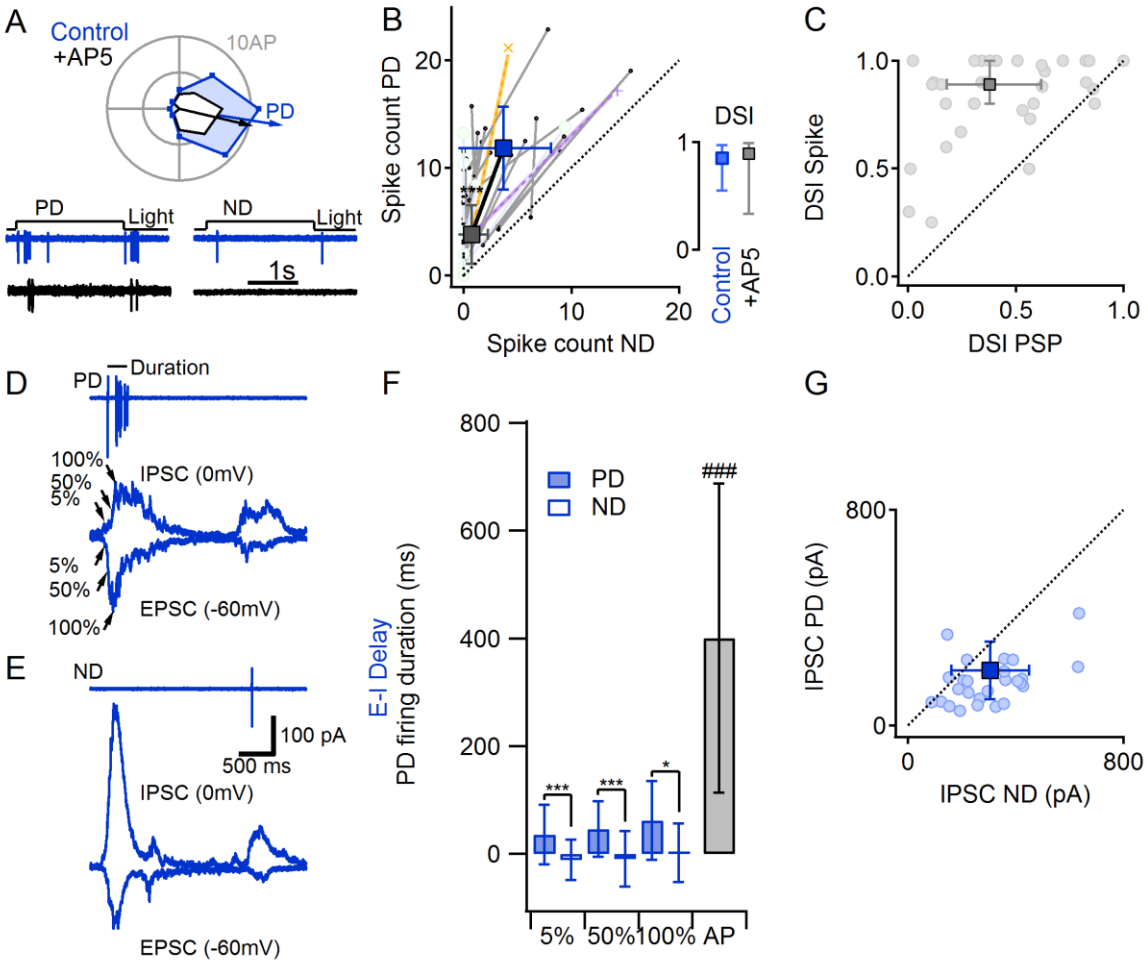

Figure S1: Sub- and Supra-threshold measurements of direction selectivity in DSGCs (related to Figure 1)

(A-C) Suprathreshold (spiking) responses in DSGCs.

(A) DS tuning curve (*top*) and individual responses (*bottom*) from a DSGC in control solution (blue) and in the presence of AP5 (black).

(B) Summary of PD and ND AP responses from 27 cells in control solution (blue) and in the presence of AP5 (black). Squares, average (±SD) of the dataset. Small symbols and gray lines indicate individual cells. Yellow ('*x*') and purple ('*+*') lines indicate theoretical multiplicative and additive scaling, respectively, of AP5 responses. *Inset*, Median DSI (±quartile).

(C) Comparison between the supra- and sub-threshold DSIs (median ± quartile; n=33 cells). $p<10^{-8}$ using Wilcoxon signed rank test for paired data.

(D-F) Temporal delay between excitation and inhibition does not play a large role in generating suprathreshold DS responses.

(D) APs (*top*) and synaptic currents (*bottom*) evoked in a DSGC by PD stimuli. Arrows indicate the time of 5%, 50% and 100% of the peak PSC amplitude. The inhibitory current is delayed compared to excitation. However, the majority of action potentials occur after the inhibition reached its peak amplitude.

(E) As in (D) for ND.

(F) While the mean (±SD) delay between excitatory and inhibitory currents is significantly larger in response to PD stimuli compared to ND (n=23 cells, *p<0.05, ***p<0.001, paired t-test), the delay difference between PD and ND is significantly less than the duration of the PD spiking responses (black, ###p<0.005 between 5%, 50% and 100% PD E-I delay, paired t-test with Bonferroni correction).

(G) IPSC amplitudes, PD vs. ND. Squares, population average (±SD, n=28). IPSCs were larger for the null direction.

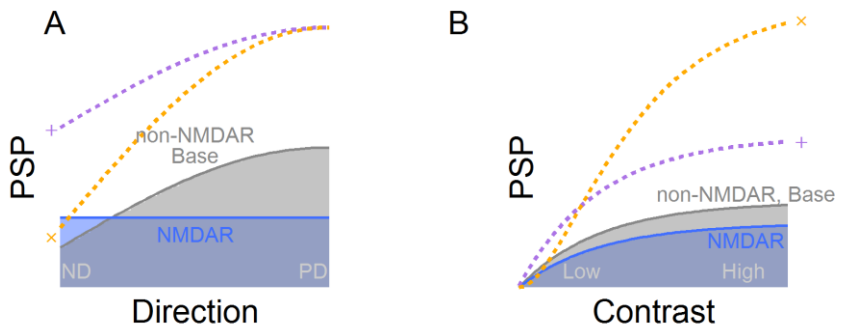

Figure S2: Comparison of different methods for investigating synaptic multiplication (related to Figure 1)
(A) Illustration of directional tuning of PSP amplitudes mediated by non-NMDAR ('base', *light gray*) and NMDAR-mediated (*blue*) components. NMDAR activation is equal in all directions because glutamate release from bipolar cells is not directionally tuned. Dotted lines indicate theoretical additive ('*+', violet*) and multiplicative ('*x', yellow*) integration of the two inputs.
Postsynaptic integration is multiplicative if the combined activation of two or more inputs results in a response that scales as a multiplicative product of the responses to the individual inputs: $\boldsymbol{R} = k\prod_{i=1}^{n} R_i$, where $\boldsymbol{R}$ is the total combined response (i.e., the PSP amplitude), R_i is the response to input *i* and *k* is a constant. Here, each input i could represent an individual synapse, or some pharmacologically distinguishable component of $\boldsymbol{R}$, i.e., the part mediated by a particular postsynaptic receptor. If we know R_i for all inputs/components and $\boldsymbol{R}$, identifying multiplication is straightforward. In many experimental systems, however, synaptic inputs/components cannot be isolated easily. In the present experiments, we separated the components of synaptic input to DSGCs into a non-NMDAR mediated component (*'base'*), measured in the presence of AP5, and an NMDAR mediated component ('*NMDAR*') that we could not measure in isolation without compromising DS computation. Because glutamate release is similar for different directional stimuli, however, we can infer the effects of the NMDAR component of the response (R_N) on $\boldsymbol{R}$ evoked by PD and ND stimuli. If NMDARs truly multiply the response to other synaptic inputs, R_N would amplify the base response (R_B) by the same factor in all directions ('×'):

$$\begin{aligned}\boldsymbol{R}_{PD} &= kR_N R_{B_{PD}} \\ \boldsymbol{R}_{ND} &= kR_N R_{B_{ND}}\end{aligned} \leftrightarrow \frac{\boldsymbol{R}_{PD}}{R_{B_{PD}}} = \frac{\boldsymbol{R}_{ND}}{R_{B_{ND}}}$$

The significant advantage of this approach is that the actual value for R_N is not required to identify synaptic multiplication.

(B) Another physiological method to vary responses in DSGCs is to change the contrast of the light stimuli. One could compare responses at two different contrasts, C_1 and C_2:

$$\begin{aligned}\boldsymbol{R}_{C_1} &= kR_{N_1} R_{B_1} \\ \boldsymbol{R}_{C_2} &= kR_{N_2} R_{B_2}\end{aligned}$$

Recall that we can experimentally determine the values of $\boldsymbol{R}_{C_x}$ and R_{B_x}, but not R_{N_x}, for each contrast level x. Since presynaptic glutamate release is not constant across different contrast conditions, $R_N(x)$ is a free parameter, making the equations unsolvable, no matter how many contrast levels are examined. In this scenario, a similar ratio (scaling) between the total combined response and the non-NMDAR component could occur for additive synaptic integration. If synaptic activation of the non-NMDAR and NMDAR channels scaled similarly across

different contrasts (i.e., so that a contrast increase that doubled the non-NMDAR drive also would double the NMDAR component), then $R_{N_x} = kR_{B_x}$ for every contrast level x. Adding the two components yields:

$$\boldsymbol{R}_{C_x} = R_{N_x} + R_{B_x} = (k+1)R_{B_x}$$

The critical distinction between varying direction and contrast is that NMDAR activation remains constant in the former but varies in the latter, precluding correct identification of synaptic multiplication.

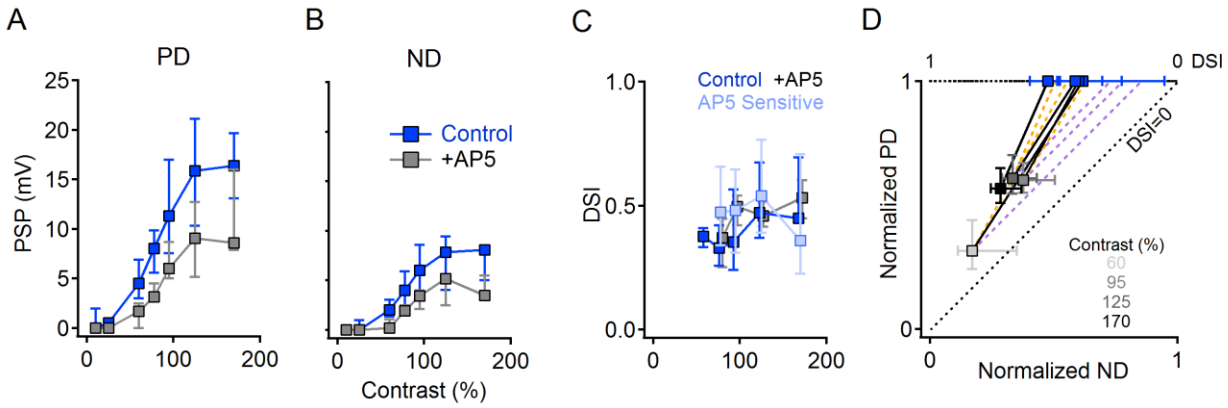

Figure S3: NMDAR mediated scaling is multiplicative for different contrast levels (related to Figure 1)

(A-B) PSP amplitudes in DSGCs grow progressively larger with increasing stimulus contrast. NMDAR blockade (black) reduced responses from control (blue) by a similar proportion at all contrast levels for which measurable responses were obtained.

(C) NMDAR blockers did not change the DSI of PSPs. Color coding as in (A and B). Light blue, AP5-sensitive component.

(D) Data from (A and B) normalized to the control PD response (median ± quartile). Yellow (‘*x*’) and purple (‘*+*’) lines indicate theoretical multiplicative and additive scaling, respectively, of the AP5 responses. NMDAR-mediated scaling follows the multiplicative trajectory for all examined contrasts.

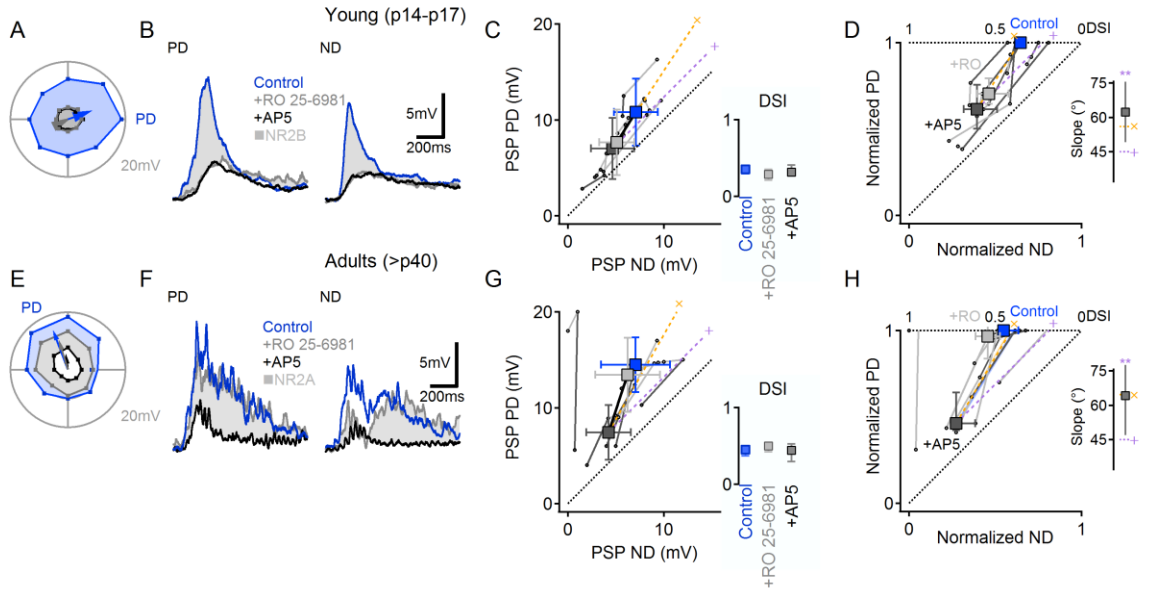

Figure S4: NMDAR multiplication persists at different developmental ages that involve different NR2 subunits (related to Figure 1)

We tested whether multiplication was robust to developmental changes in NMDAR subunit expression, as DRD4^{+} DSGCs express synaptic NR2B-containing NMDARs prior to P21, but not at later time points (Stafford et al., 2014). (A) Subthreshold directional tuning of a DSGC from a P14 retina. The NMDAR component was mediates almost entirely by NR2B containing NMDARs, blocked with the NR2B-specific NMDAR antagonist Ro 25-6981 (see legend in B).

(B) PSPs evoked by PD (*left*) and ND (*middle*) stimuli from the cell in (A).

(C) Summary of control (blue), RO 25-6981 (grey) and AP5 (black) responses in 7 cells. Squares, average (±SD) of the dataset. *Inset*, median DSI (± quartile). Yellow ('*x*') and purple ('*+*') lines indicate theoretical multiplicative and additive scaling, respectively, of the AP5 responses.

(D) Data in (C) normalized to the control PD response in each DSGC. *Inset*, The mean slope of NMDAR scaling follows the expected multiplicative trend. The mean slope is not dissimilar from multiplication, but significantly different from addition ($p<0.01$). Error bars, confidence interval of 99%.

(E-F) As in (A and B) for PSPs from P70 animal.

(G-H) As in (C and D) from adult (>P40) animals (n=7 cells). Although Ro 25-6981 exerted little effect on PSPs in adult DSGCs, subsequent application of AP5 indicated that non-NR2B NMDARs mediate multiplication in adult retina.

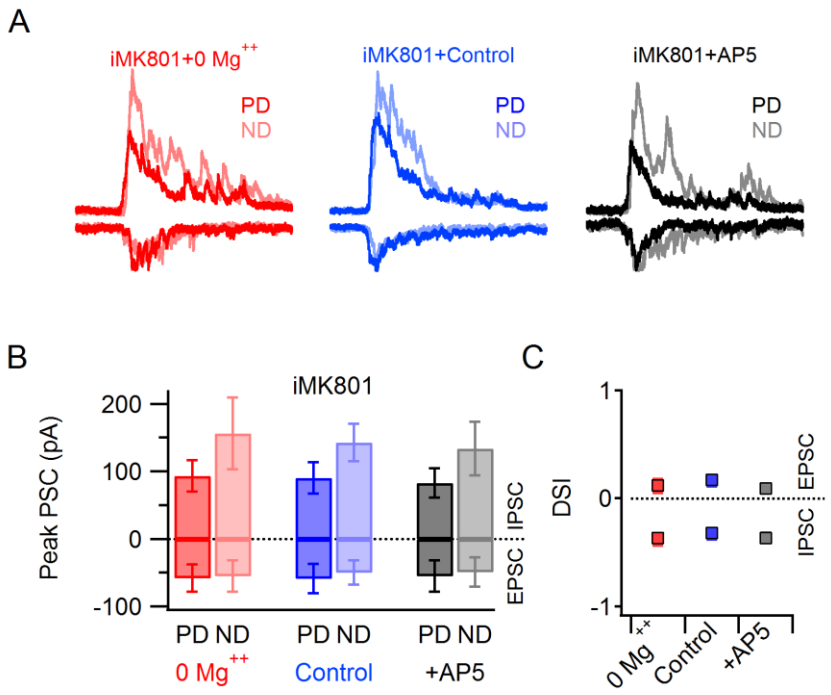

Figure S5: Light evoked responses in presynaptic DS circuitry are not affected by experimental manipulations of NMDARs (related to Figures 2 and 5)

(A) Example EPSCs (V_{hold}=-65 mV) and IPSCs (V_{hold}=0 mV) for PD (bold trace) and ND (light trace) stimuli in Mg^{++}-free extracellular ACSF (red, left), control ACSF (blue, center) and control ACSF with 50 µm AP5 (black, right).

(B) EPSC and IPSC amplitudes in ND and PD from 6 DSGCs. Responses were not significantly different in the three extracellular solutions tested ($p>0.2$ paired t-test with Bonferroni correction for multiple comparisons).

(C) DSI values were similar between experimental conditions ($p>0.5$ and $p>0.3$ Wilcoxon signed rank test with Bonferroni correction for multiple comparisons between excitatory and inhibitory drives, respectively). DSIs were negative for IPSCs because IPSCs in DSGCs are larger in response to ND stimuli.

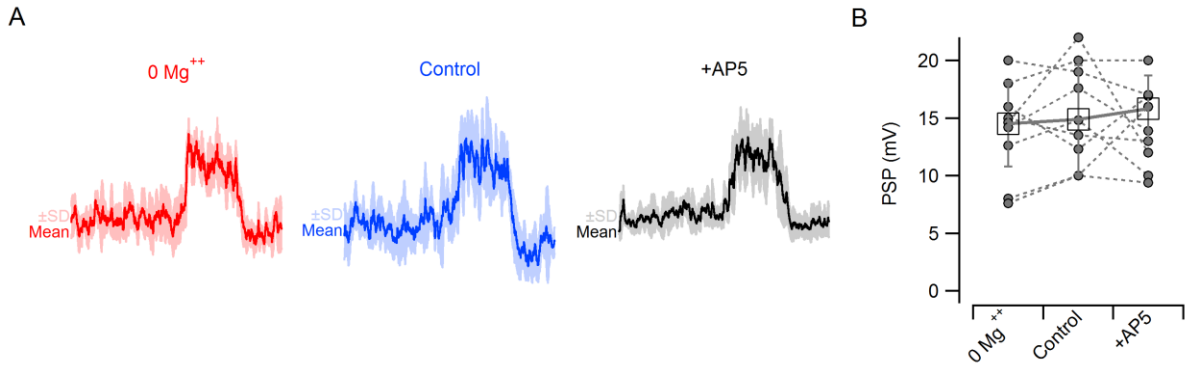

Figure S6: SAC light responses are not affected by manipulation of NMDARs (related to Figures 2 and 5)

(A) Light evoked PSPs (bold-mean; shaded-SD for 5 repetitions, all traces from the same cell) from a SAC in Mg^{++}-free ACSF ('0 Mg^{++}', red), 1 mM Mg^{++} ('Control', blue) and 1 mM Mg^{++} + 50 µm AP5 ('+AP5', black). Responses were evoked by the same (noise-free) motion stimuli used to elicit DS responses in DSGCs (see Experimental Procedures).

(B) Summarized PSP amplitudes from 9 SACs in different experimental conditions. No significant differences were detected ($p>0.2$, paired t-test with Bonferroni correction for multiple comparisons).

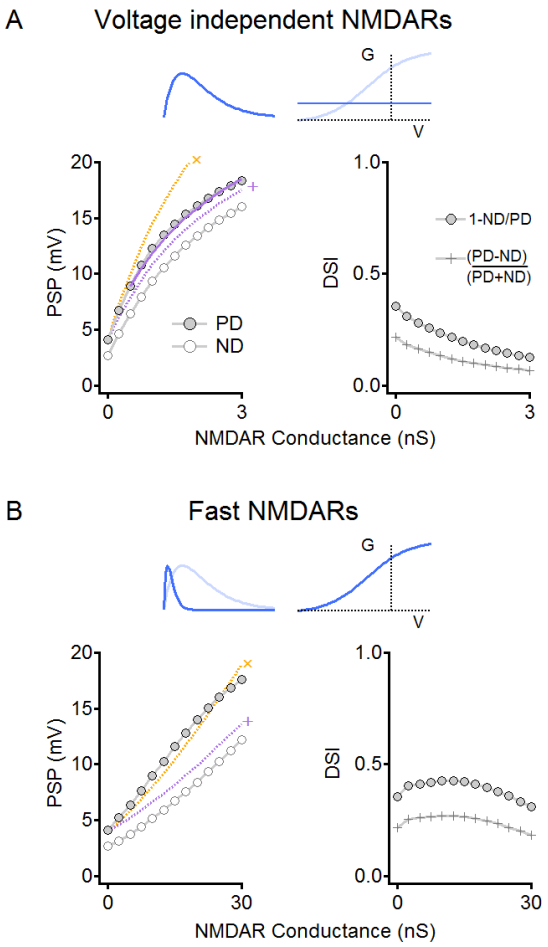

Figure S7: Characteristic voltage dependence, not time course, of NMDAR conductance is required for multiplicative scaling (related to Figure 5)

Simulated NMDAR amplification for directionally tuned inhibition, with similar baseline parameters as in Figure 5.

(A) Scaling by voltage-independent (ohmic) NMDARs. *Left*, PSP peak values scale additively with increasing NMDAR conductance. Yellow ('*x*') and purple ('*+*') lines represent theoretical multiplicative and additive scaling, respectively, of the baseline responses. Solid purple trace marks theoretical additive amplification of 9 mV PD PSP. *Right*, increasing NMDAR conductance reduced DSI values. *Insets*, temporal shape (*left*) and the voltage dependence (*right*) of the simulated NMDAR conductance.

(B) Scaling is multiplicative for voltage-dependent NMDARs with faster kinetics matching those of AMPARs.

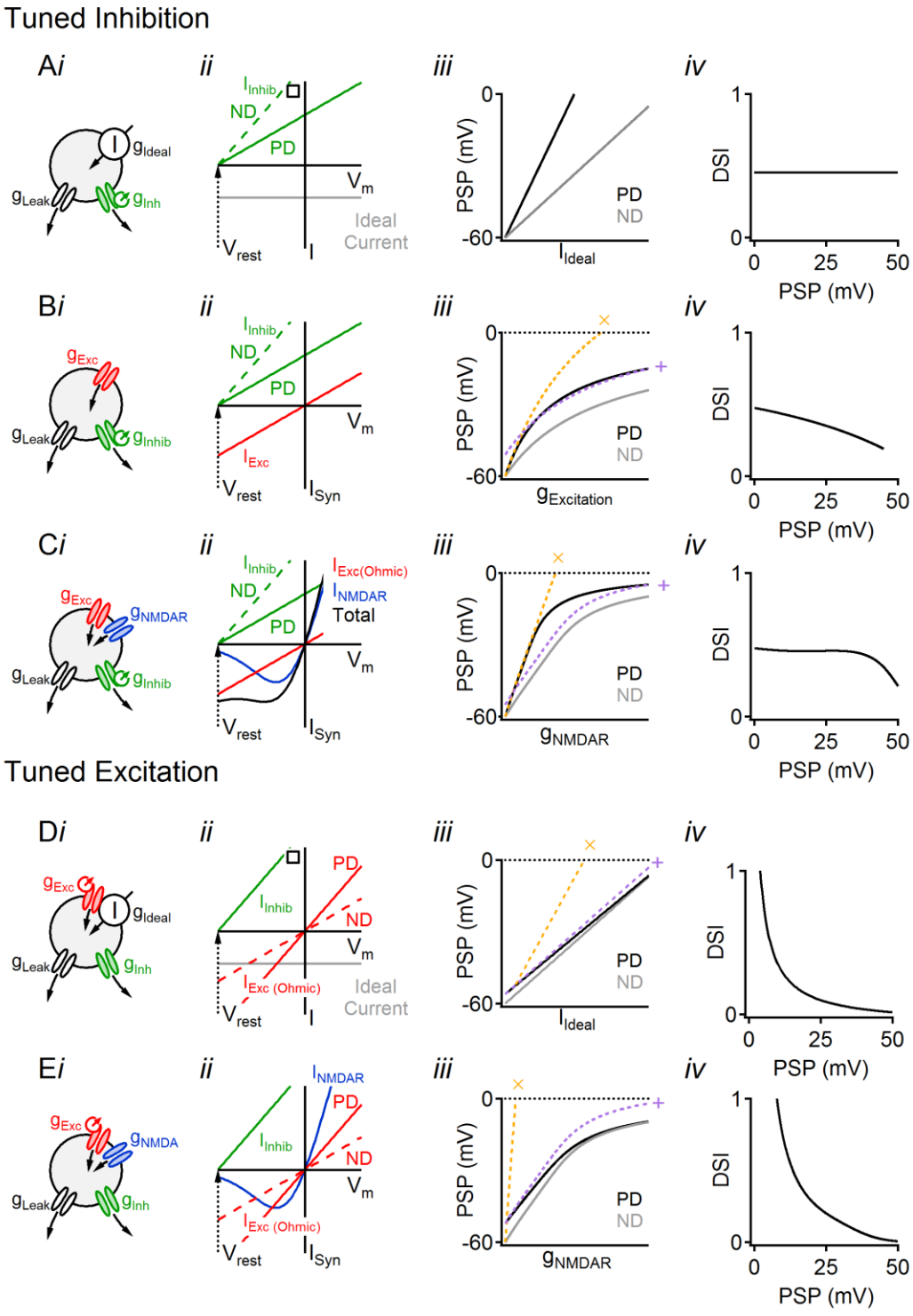

Figure S8: Mechanisms underlying NMDAR multiplicative scaling (related to Figures 3-5)

Synaptic interactions were examined in a simplified, single-compartment, passive membrane model with a leak conductance g_{Leak} and no other voltage gated channels. All synaptic conductances exhibited the same (square

wave) time course. In each condition, we show: (*i*) a schematic of the simulated inputs to the cell; (*ii*) the I:V relationship of the ideal (grey), Ohmic excitatory (red), NMDAR (blue) and inhibitory (green) synaptic currents; (*iii*) PSP amplitude in response to PD (black) and ND (grey) activation as a function of the magnitude of the amplifying excitatory drive (expected additive and multiplicative scaling are indicated by purple ('+') and yellow ('x') lines, respectively); and (*iv*) calculated DSI values vs. different PD PSP amplitudes.

(**A-C**) Tuned inhibitory drive scheme in which the ND inhibitory conductance is larger (*i*, green). For simplicity, assume that inhibition is shunting ($E_{rev}=E_{rest}$=-60mV). Accordingly, changing the inhibitory drive modifies the resistance of the cell, R_{IN} ($R_{IN}=1/g_{Total}=1/(g_{Leak}+g_{Inhib})$), and thus the input resistance is lower in response to ND activation.

(**A**) An ideal current (i.e., constant across all membrane potentials) scales the responses multiplicatively in the tuned inhibition DS model. The PSP experienced by the cell will follow Ohm's law, $PSP=I\times R_{IN}$. When plotted as a function of the magnitude of the excitatory current (I_{Ideal}), the PSP amplitude follows a line that goes through the origin and has a slope of R_{IN} (*iii*). Therefore, for all ideal current levels the ratio between PD and ND PSPs is constant (the inverse ratio of the corresponding input resistances), corresponding to invariable DSI values across all membrane potentials (*iv*).

(**B**) Ohmic excitatory synaptic conductances, such as those mediated by AMPARs or nAChRs, do not mediate multiplicative scaling. Because depolarization from rest reduces the driving force of the excitatory conductances, PSP amplitude varies sublinearly with synaptic conductance (*iii*). By lowering the input resistance, shunting inhibition reduces PSP amplitude, but the consequent increase in driving force reduces the impact of inhibition on larger PSPs (*iii*), leading to a decrease in DSI at larger $g_{Excitation}$ values (*iv*).

(**C**) An NMDAR conductance can significantly extend the multiplicative region in the tuned inhibition DS model. Unlike the Ohmic conductance, the conductance of NMDARs increases with postsynaptic voltage. The combination of Ohmic and NMDAR conductances can approximate an ideal current source over a substantial voltage range (*ii*, black), Consequently, synaptic input with an NMDAR component enables multiplicative scaling (*iii*) and conserved DSI over a wide potential range (*iv*).

(**D-E**) In the excitatory DS tuning model, directional tuning is encoded by the magnitude of an Ohmic excitatory synaptic drive. The total synaptic conductance is larger (and, consequently, the input resistance is lower) in response to PD activation.

(**D**) Scaling by an ideal current source. As before, the degree of scaling by the ideal current depends on the input resistance. However, unlike in the case of tuned inhibition (**A**), the ideal current contributes less to PD PSP. Eventually, the PD and ND responses converge.

(**E**) Scaling with NMDARs in the tuned excitation DS scheme. Simulations show that the contribution of the larger NMDAR PD conductance (due less Mg^{++} block during larger PD PSPs) is offset by the effects of the reduced input resistance. The resulting NMDAR-mediated scaling is nearly additive for g_{NMDAR} values, and becomes sub-additive for stronger g_{NMDAR}.

SUPPLEMENTARY EXPERIMENTAL PROCEDURES

Recording procedures

Extracellular solution was Ames (Sigma) equilibrated with 95% O_2/5% CO_2 for all experiments except those examining the effects of removing Mg^{++}. In those experiments, control artificial cerebrospinal solution (ACSF) was composed of the following: 120 mM NaCl, 3 mM KCl, 0.75 mM $CaCl_2$, 1 mM $MgCl_2$, 6 mM Glucose, 0.5 mM KH_2PO_4, 0.05 mM L-Glutamine, 0.02 mM ascorbic acid 0.01 mM myo-Inositol. Mg^{++}-free solution was identical to control except that $MgCl_2$ was omitted. Somatic recordings were obtained with an Axopatch 700B amplifier (Molecular Devices), low-pass filtered at 4 kHZ (Bessel) and digitized at 20–50 kHz with an Instrutech ITC-18 A/D board (HEKA Elektronik) controlled by custom acquisition software written in IgorPro (WaveMetrics). Patch pipet (4-6MΩ) solution depended on the experiment: When only cell-attached recordings were required, pipets were filled with Ames solution (Sigma). For voltage clamp: 90 mM $CsCH_3SO_4$, 20 mM TEA-Cl, 10 mM HEPES, 10 mM EGTA, 10 mM phosphocreatine disodium salt hydrate, 4 mM Mg-ATP and 0.4 mM Na-GTP; For current clamp: 110 mM K-$MeSO_4H$, 10 mMNaCl, 5 mM HEPES,4 mM Mg-ATP and 0.4 mM Na-GTP, 2 mM EGTA. In some experiments EGTA was replaced with 0.2 mM OGB-1. For current clamp with elevated internal chloride: 55 mM K-$MeSO_4H$, 55 mM KCl, 10 mM NaCl, 5 mM HEPES,4 mM Mg-ATP and 0.4 mM Na-GTP, 2 mM EGTA (calculated E_{Cl}~-20 mV). NMDARs were blocked with D-AP5 (50 µM, Sigma-Aldrich) or MK801 (10 µM, Sigma-Aldrich); both blockers exerted similar effects on light-evoked responses, and the experiments were pooled for analysis. Sodium channels were blocked extracellularly with tetrodotoxin (1 µM, Ascent Scientific) or intracellularly with QX 314 (10 mM, Sigma-Aldrich) added to the pipet solution.

Light stimulation

Photon flux was measured at the focal plane of the photoreceptors using a DR-2000 radiometer (Gamma Scientific) and converted to photoisomerizations per rod assuming a collecting area of 0.5 μm^2 (Field and Rieke, 2002) the resulting background light intensity was ~30,000 R* rod^{-1} sec^{-1}. Unless otherwise noted, stimuli consisted of bright (30,000-115,000 R* rod^{-1} sec^{-1}) rectangles (500µm x2000 µm) moving at 1 mm/sec along the long axis in 8 different directions, and were presented at 10-15 s intervals. Stimuli were restricted to a 2 mm x 2 mm area on the retina centered on the recorded cell. Weber contrast (C_w) between the luminance of the bar (φ_{stim}) and the background (φ_{bkgd}) was calculated as $C_w = (\varphi_{stim} - \varphi_{bkgd})/\varphi_{bkgd}$. Except where noted, stimulus contrast was 170%. For elevated chloride experiments we routinely reduced the contrast to 80-120% to limit control PSP amplitudes below 20 mV.

When noisy visual stimuli were delivered, the degree of noise was set by independent variation of the background and the moving bar light intensity. At each frame a new value for both variables (background, stimulus) was picked from two Gaussian distributions of light intensity, in which the variability (variability=[SD/(background luminance)]*100) set the noise level and the mean corresponded to the original

(noise free) intensity of the background and the stimulus, respectively. 0% (no noise), 25%, 50% and 100% variability levels were used. As the display intensity was found not to be a linear function of pixel values, to preserve the mean contrast at all noise levels, the new light intensity was converted into pixel value based on an offline calibrated lookup table.

Targeting DSGCs

DRD4 DSGCs were identified by their GFP expression using a Zeiss LSM-510 multiphoton microscope. Two photon excitation (820 nm) was provided by a mode locked Ti:S laser (Chameleon, Coherent). Fluorescence was acquired between 500-550 nM with confocal descanned photomultiplier tube.

Data analysis

We first determined the preferred direction for each DSGC by recording (cell-attached) AP responses to the onset of light bars moving in 8 different directions. We then computed the angle of the vector of the average response, and designated the closest of the 8 directions to be the preferred direction (PD); the opposite direction was designated as null (ND). For AP recordings, responses were quantified by the number of action potentials in the ON (leading bar edge) response. For subthreshold recordings, we measured the ON-stimulus evoked mean peak depolarization (current clamp) or peak current (voltage clamp), unless noisy visual stimulus was used, in which case we measured the mean PSP amplitude over a 100 ms window around the peak. DSI was calculated as (PD response-ND response)/PD response, where PD response and ND response are the responses to light bars moving in the PD and ND, respectively. In several instances we compared the result of this DSI calculation with an alternative formula: DSI = (PD response-ND response)/(PD response+ ND response). Both measures of DSI remain constant when PD and ND responses are multiplied by the same scalar value. We opted to use the former equation, as it accommodates negative ND responses (sometimes observed in PSP recordings) better and is more sensitive to changes in the low DSI values that are more frequently encountered in PSP recordings.

To compare the effects of NMDAR blockers on PSP amplitude, we normalized the ND PSPs and PSPs recorded with NMDARs blockers to the peak PSPs for PD control conditions. A divisive effect of NMDAR blockers would reduce responses proportionally in all directions: on a plot of PD responses vs. ND responses, points would fall along a line connecting control responses to the origin. A subtractive effect of NMDAR blockers would reduce the PDR and NDR equally, with responses falling along a line with a slope of 1 that goes through the control data point.

In internal MK801 experiments we examined the PSP before (<5 min following break in) and after (20-30 min after break) MK801 blockade of NMDARs.

Receiver operating characteristic (ROC) and accuracy classification tests

The ROC performs a binary classification test based on the following confusion matrix:

	True condition

Predicted condition	Signal	Noise	
Signal	**True Positive (TP)**	False Positive (FP)	ROC
Noise	False Negative (FN)	**True Negative (TN)**	

Accuracy

TP and FP rates are required to compute the ROC test (shaded). We derived these rates from the cumulative distribution of the recorded responses over the membrane potentials (subthreshold) or spike count (suprathreshold). We computed the distribution of the responses within a 500 ms window over the PD, ND and baseline responses (the latter where selected to be between 2.5 seconds before stimulus presentation). Results from 3-10 repetitions in each experimental condition or from all four visual noise levels were summed together. When normalized to one, the resulting distribution of the responses recorded during the PD stimulation represent the TP rate, and the distribution of the responses recorded during the baseline or ND epochs represent the FP rates. The ROC space is defined as the TP rate vs. the FP rate. Intuitively, the resulting curve depicts the result of the confusion matrix for the range of membrane potentials or spike counts. The area under the ROC curve provides readout of how well the two distributions can be discriminated. This area ranges between 0.5 (identical distributions) to 1 (no overlap, perfectly separated distributions).

Because the ROC analysis does not provide information on the location of optimal discrimination (on a membrane potential axis), we also used an accuracy test. The accuracy test was conducted on the same set of subthreshold data as ROC analysis. The test measures the percent of correctly classified responses (TP + TN, bold) vs. the entire population (incorrectly and correctly classified responses, TP+TN+FP+FN) for a given voltage threshold. Like the ROC, the analysis test can range from 0.5 (chance) and 1 (perfect classification). The shape of the accuracy curve over the membrane potential provides the degree of accurate classification for a range of thresholds. We used the area under the curve to obtain an estimate of the precision of the suprathreshold responses (assuming that a wider potential range with a good accuracy produces better discrimination). As the results from the accuracy test varied substantially between different cells due to the difference in the absolute amplitude of the responses, we normalized the area under the accuracy curve of the responses recorded with zero extracellular magnesium and control magnesium levels by the area under the accuracy curve of the responses recorded after NMDAR blockage with AP5.

Unless otherwise stated, statistical significance was calculated with the Mann–Whitney U test, significance was concluded when $p<0.05$. Bonferroni correction for multiple comparisons was used when more than one comparison was made. To ease the presentation of the data, we multiplied the calculated p-value by the number of comparisons while keeping the significance level constant, which is equivalent to the original definition of Bonferroni correction, which is a reduction of the significance level by the number of comparisons.

Simulation

One of the recorded DSGC was imaged and reconstructed using ImageJ plugin 'Simple Neurite Tracer' and converted into a multi-compartmental model (121 on-; 119 off-stratifying dendritic segments) constructed with NEURON simulation software and run on the Biowulf Linux cluster at the National Institutes of Health (http://biowulf.nih.gov). Multicompartmental numerical simulations were performed in the NEURON simulation environment (Hines and Carnevale, 1997). The distribution and parameters of the passive and active conductances were set to match values derived from DSGC recordings: The membrane capacitance and resistance were 1 $\mu F/cm^2$ and $10^4\ \Omega cm^2$, respectively. Axial resistance was 100 Ωcm. The leak current across the membrane resistance had a reversal potential of -60 mV. We matched the firing rate of experimentally recorded somatic current injections with the following distribution of voltage gated channels at DSGC soma/dendrties (peak conductance in mS/cm^2); sodium (200/2), fast potassium rectifier (70/7), Delayed rectifier (3/0). The reversal potential for sodium and potassium was set to 50 mV and -77 mV, respectively. For voltage clamp simulations we eliminated voltage-gated conductances and set the membrane resistance to $10^5\ \Omega cm^2$. In DSGC recordings, we observed that activation of voltage-gated channels in response to a step current injection introduced significant membrane potential variability; to simulate the effect of channel noise in the model, we included stochastic behavior in the description of state transitions for each channel (Linaro et al., 2011). All simulations were 1.2 s duration (0.1 ms time step). 100 trials were conducted for each simulated condition.

Simulated light responses

The simulated DS network consisted of 282 bipolar cells and SACs, each innervating the nearest On DSGC dendrite. Presynaptic cells were modeled as point sources located at the middle of the innervated branch. Light activation was simulated by a 1 mm long rectangular area moving at 1 mm/s over the network. When the leading edge of the stimulus overlapped with the position of a presynaptic cell, the cell became depolarized to a new potential with a rise time of 50 ms and a decay time of 200 ms. Each presynaptic synapse had a readily releasable pool (RRP) of 10 vesicles (Singer and Diamond, 2006), which could be released every 1 ms with a probability of release dependent on the membrane potential. Vesicles then could be replenished from an infinite vesicle pool at a rate of 500 ms^{-1} (Singer and Diamond, 2006). The amplitude of the stimulus induced depolarization was set to deplete, on average, 30% of the RRP. The level of presynaptic depolarization was varied in each presynaptic cell with a variance of 10% of the mean for bipolar cells and 20% for SACs (unpublished observations). To simulate DS tuning of GABAergic inputs, we reduced the peak depolarization to ND stimuli for the GABAergic drive by 66% compared to PD and bipolar activation. To simulate directionally tuned excitation we increased the cholinergic drive by a factor of 4 for PD. Simulation of both tuned excitation and inhibition was conducted by increasing the cholinergic drive two fold and reducing the GABAergic input by a factor of 2 between PD and ND stimulations. For simulations with elevated E_{Cl} the mean depolarization of presynaptic cells was set to 30% of the control values to match experimental results.

Simulated synaptic release

We simulated three distinct classes of synapses that activated different postsynaptic receptors: 1) Glutamatergic inputs from bipolar cells, which activated NMDARs and AMPARs. NMDARs had a rise time of 2 ms, decay time of 60 ms and a peak unitary conductance of 2 nS which was voltage dependent as following: $NMDA_G = \frac{1}{(1+0.25[Mg^{++}]e^{(-0.07v)})}$ where [Mg^{++}] is the extracellular magnesium concentration (1.2 mM for control conditions, results were consistent over a 0.5-1.5 mM range) and v is the membrane potential of the postsynaptic dendrite (Jahr and Stevens, 1990). AMPARs had an instantaneous rise time, decay time of 2 ms and unitary conductance of 1 nS. 2) Cholinergic inputs from SACs, which activated nicotinic Ach receptors with an instantaneous rise time, decay time of 3 ms and a unitary conductance of 2nS. Excitatory conductances reversed at 0 mV. 3) GABAergic inputs from a distinct vesicular pool in SACs. GABARs were activated with an instantaneous rise time, 30 ms decay time, 2 nS conductance and a reversal potential of -60 ms.

Single compartment simulation

For simulations shown on Figure S8, a passive (with membrane capacitance of 1000 Ωcm^2), single compartment (length and diameter of 3µm) model was simulated in NEURON. Simplified synaptic inputs in the model had no temporal dynamics (for activation/deactivation). Instead, synaptic drives were activated between 50 to 150 ms, during which time the simulation approached the voltage steady state based on the I-V dependence of the synaptic conductances. The following currents were used: 1) Ideal current, with a constant current across all voltages. 2) $GABA_A$R-like current with an ohmic conductance of 1nS reversing at -60 mV, which was also the resting potential of the cell 3) nAChR- or AMPAR-like ohmic conductance with a reversal potential of 0 mV 4) NMDAR-like current with the voltage dependence specified above and reversal potential of 0 mV. Directional tuning was modeled as either a two fold increase in inhibitory conductance at ND (tuned inhibition), or an additional 0.1nS ohmic excitatory conductance at the PD (tuned excitation). The peak PSP amplitudes were used to calculate the DSI values. The following synaptic configurations were tested: A) Ideal and inhibitory currents B) AMPAR and inhibitory currents C) AMPAR+NMDAR and inhibitory currents. In each configuration the simulation was repeated over a range of excitatory conductances. Expected multiplicative and additive curves were calculated from synaptic combination which produced PD responses of ~10 mV.

SUPPLEMENTARY REFERENCES

Field, G.D., and Rieke, F. (2002). Nonlinear signal transfer from mouse rods to bipolar cells and implications for visual sensitivity. Neuron 34, 773-785.
Hines, M.L., and Carnevale, N.T. (1997). The NEURON simulation environment. Neural computation 9, 1179-1209.
Jahr, C.E., and Stevens, C.F. (1990). Voltage dependence of NMDA-activated macroscopic conductances predicted by single-channel kinetics. The Journal of neuroscience : the official journal of the Society for Neuroscience 10, 3178-3182.
Linaro, D., Storace, M., and Giugliano, M. (2011). Accurate and fast simulation of channel noise in conductance-based model neurons by diffusion approximation. PLoS Comput Biol 7, e1001102.

Singer, J.H., and Diamond, J.S. (2006). Vesicle depletion and synaptic depression at a mammalian ribbon synapse. Journal of neurophysiology 95, 3191-3198.
Stafford, B.K., Park, S.J., Wong, K.Y., and Demb, J.B. (2014). Developmental Changes in NMDA Receptor Subunit Composition at ON and OFF Bipolar Cell Synapses onto Direction-Selective Retinal Ganglion Cells. J Neurosci 34, 1942-1948.